Assessment of Area-Average Absorbed Power Density on Realistic Tissue Models at mmWaves

Ante Lojić Kapetanović
FESB
Univ Split
Split, Croatia
alojic00@fesb.hr

Giulia Sacco
IETR – UMR 6164
Univ Rennes, CNRS
Rennes, France
giulia.sacco@univ-rennes1.fr

Dragan Poljak
FESB
Univ Split
Split, Croatia
dpoljak@fesb.hr

Maxim Zhadobov
IETR – UMR 6164
Univ Rennes, CNRS
Rennes, France
maxim.zhadobov@univ-rennes1.fr

2022 IEEE MTT-S International Microwave Biomedical Conference (IMBioC) | 978-1-6654-2340-3/22/$31.00 ©2022 IEEE | DOI: 10.1109/IMBIOC52515.2022.9790150

***Abstract*—Currently, most state-of-the-art research in computational dosimetry utilizes flat-surface tissue models to simplify the problem geometry and thus mitigate computational complexity. However, depending on the ratio of the penetration depth and the curvature radius, this may lead to a non-correct estimation of the power absorbed by the tissues due to constructive/destructive interference. In this study, we propose an accurate evaluation of the area-average absorbed power density in curved tissue-equivalent models by computing the surface integral of the normal component of the absorbed power density vector field. The numerical analysis is performed for plane wave exposure of an ear model at 60 GHz. We also investigate the effect of the averaging area shape on the absorbed power density by considering 1 cm^2 square- and disk-shaped averaging surfaces. Results show a substantial relative difference of 14 % in the area-averaged absorbed power density over a disk-shaped averaging surface between transverse electric and magnetic polarization, with the reference being the value of the area-averaged absorbed power density for a planar homogeneous model and normal incidence. By using the same reference value, negligible differences of 1.81 % and 0.92 % for transverse electric and magnetic polarization, respectively, are present when the averaging area shape changes. According to the studied exposure scenarios, the area-averaged absorbed power density variations as a function of the averaging surface geometry are less significant than those related to the polarization of the incident field.**

***Index Terms*—computational dosimetry, millimeter wave exposure, ear model, absorbed power density**

I. Introduction

With increasing need for higher data rates, more reliable wireless connection and improved latency, millimeter waves (mmW) spectrum represents a promising solution. International guidelines [1] and standards [2] for human exposure to electromagnetic (EM) fields have recently undergone major revisions given the massive breakthrough of the 5$^{\text{th}}$ generation (5G) heterogeneous cellular network technology. One of the most prominent updates is the introduction of a novel basic restriction metric at frequencies above 6 GHz - the absorbed power density (APD), which represents the power per unit area deposited over irradiated surface of the tissue.

Between 6 GHz and 30 GHz, the APD is averaged over a square of 4 cm^2 to account for the consistency with the volume-average specific absorption rate (SAR) at lower frequencies. The validity of such an approach has been established in thermal modeling study by Hashimoto et al. [3]. As the additional criterion imposed above 30 GHz (and less than 300 GHz), the APD averaged over 1 cm^2 should not exceed 2 times the value for the square 4 cm^2 averaging area.

At present, the majority of the computational dosimetry research dealing with human exposure at mmW is using simplified, canonical, most often planar tissue-equivalent phantoms [4]. Some efforts have been made to take into account more realistic models with non-planar surfaces, e.g., in [5] where simplified structures having a diameter equal or longer than the side of the square typically used to average the APD (2 cm^2) have been considered. The effect of curvature in structures with smaller radii (i.e., finger and ear) was investigated in [6].

As a continuation of this work, we propose a simple and accurate method to evaluate the area-averaged absorbed power density (APD_{av}) over a curved, realistic surface at mmW. The impact of the shape of the averaging surface is considered and placed in the context of exposure guidelines and standards.

II. Materials and Methods

A. Electromagnetic Simulation Setup

A realistic ear model, Fig. 1, is considered for the EM simulation. The model dimensions are set to match the average size of the ear of a middle-aged adult [7]. The electric and magnetic field distribution over the model surface are computed with the finite element method by using the Frequency Domain Solver implemented in CST Studio Suite. A plane wave oriented along the z-axis at 60 GHz of both transverse electric (TE) and transverse magnetic (TM) polarization is used as source. The complex permittivity of the ear is set to 7.98 - j10.90 corresponding to the dry skin of an adult [8]. The model is discretized with a tetrahedral mesh, and the maximal size of a mesh cell is set to $\lambda/8$ (15 million cells in total). Perfectly matched layers are used as boundary conditions in all directions to simulate the open space conditions.

This research has been supported by the European Regional Development Fund under the grant KK.01.1.1.01.0009 (DATACROSS), the French National Research Program for Environmental and Occupational Health of ANSES under Grant 2018/2 RF/07 through the NEAR 5G Project, and has also received funding from the European Union's Horizon 2020 research and innovation programme under the Marie Skłodowska-Curie grant agreement N° 899546.

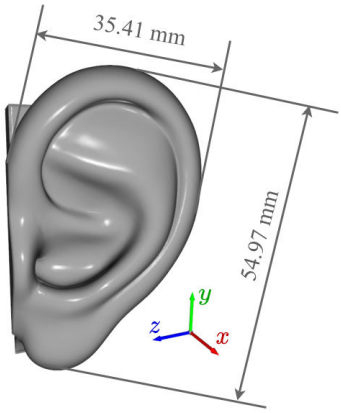

Fig. 1: Computational model of an ear.

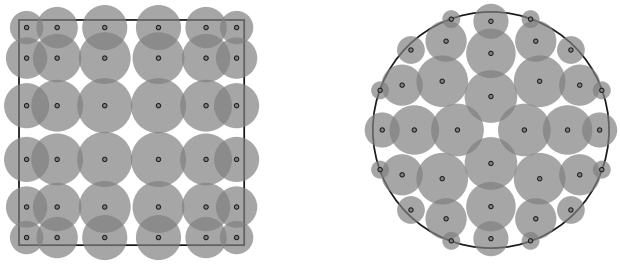

(a) Square-shaped domain. (b) Disk-shaped domain.

Fig. 2: Spatial distribution of integration nodes (dots) used for the assessment of the APD_{av} on the surface of the ear. Radii of each small circle surrounding nodes represents corresponding integration weights.

B. Assessment of Area-Average Absorbed Power Density

The APD_{av} is defined as the spatial average of the normal component of the time-averaged Poynting vector [1]:

$$APD_{\text{av}} = \frac{1}{2A} \iint_A \Re\big[\boldsymbol{E} \times \boldsymbol{H}^*\big] \cdot \boldsymbol{n} \, \mathrm{d}A \tag{1}$$

where $\boldsymbol{E}$ and $\boldsymbol{H}^*$ are the complex electric field and complex conjugate magnetic field, respectively, and $\boldsymbol{n}$ denotes the unit normal vector field spatially distributed over the irradiated surface of area A.

Components of the unit vector field normal to the surface of a model are evaluated numerically by utilizing the principal component analysis (PCA)-based method proposed in [9] at each point in which the EM power density is computed. Firstly, the local neighborhood of a point is located within some fixed, predefined scale factor, e.g., a number of neighbors, k, for k-nearest neighbors algorithm. A local tangent plane is then estimated via PCA regression - by computing the eigenvectors and eigenvalues of a covariance matrix created from the local neighborhood of a query point. The components of the normal vector thus defined are not consistently oriented over an entire point cloud due to the nature of PCA. Therefore, the last step is to propagate the orientation to adjacent planes in the Riemann graph starting from a desired viewpoint, in this case, with respect to the direction of a plane wave propagation.

The assessment of the APD_{av} by approximating the surface integral in Eq. (1) is obtained as the weighted dot product between the corresponding components of the EM power density vector field and the unit normal vector field. Two integration schemes are considered, namely the 6^{th} degree 2-dimensional Gaussian-Legendre quadrature for a squared domain, and the 12^{th} degree symmetric quadrature formula for a unit disk [10]. Integration degree is chosen to obtain the same level of spatial complexity, i.e., the number of sampled nodes and associated weights, for both domains. For a squared domain, nodes are selected as roots of the $n = 6$ degree Legendre polynomial defined to allow the quadrature rule to integrate degree $2n - 1 = 11$ polynomials exactly, while weights are derived for each corresponding node [11]. The distribution of integration nodes is shown in Fig. 2 where each black dot corresponds to an integration node position, and radii of shaded circular regions surrounding nodes represent (normalized) integration weights derived from the underlying orthogonal polynomials.

III. Results and Discussion

According to the specification in [1], the surface for spatial averaging of the APD is set to 1×1 cm^2 in addition to 2×2 cm^2 for EM exposure above 30 GHz. In the following example, we investigate how the shape of the averaging surface and the polarization of a plane wave impacts the APD_{av}. Two geometries are considered: a square of 1 cm^2, and a disk with a radius of 0.56 cm resulting in the surface area of ~1 cm^2. Given the width of an ear model (x-axis) is slightly thicker than 1 cm and that the most exposed area (worst case scenario) is approximately 1 cm^2, averaging surfaces of 4 cm^2 area are not considered in the analysis. Both averaging surfaces considered in this study have the same center point and are placed at the most irradiated region of the ear, which is found by computing the APD_{av} for all points on the directly exposed surface.

The leftmost and the center view in Fig. 3 show the distribution of the normal component of the real part of the time-averaged Poynting vector in TE mode, while the two scatter diagrams on the right zoom in to a square- and disk-shaped parametrized surfaces for the computation of the APD_{av}. Identical analysis is also performed in TM mode. For the sake of brevity, the APD distribution for TM polarization is not shown in Fig. 3 but the results are summarized in Table I. Even though the relative difference in APD_{av} for different surfaces and the same polarization is within 2 % (1.81 % for TE and 0.92 % for TM), the comparison between TE and TM mode indicates substantial deviations of 13.11 % and 14 % for square- and disk-shaped parametrized surfaces, respectively. The APD_{av} reference is defined as the value for a planar homogeneous model and normal incidence and it equals to 6.22 W m^{-2}. The maximal value of the APD_{av} is 5.73 W m^{-2} for the case of a TE polarized plane wave and disk-shaped averaging surface.

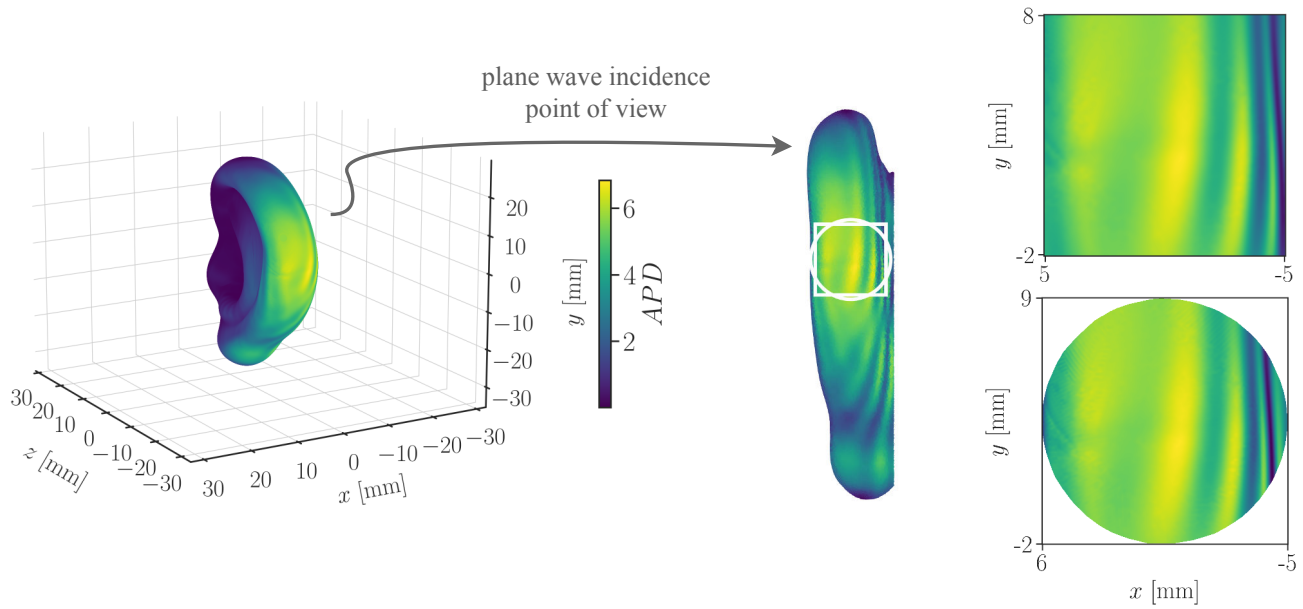

Fig. 3: APD distribution over the surface of the ear exposed to a TE plane wave.

TABLE I: Results summary.

APD_{av} [W m^{-2}]		averaging surface shape		rel. % difference
		square	*disk*	
polarization	*TE*	5.61	5.73	1.81
	TM	4.80	4.85	0.92
rel. % difference		13.11	14	

IV. Conclusion

We proposed a novel approach to assess the APD_{av} over irregular, non-planar tissue surfaces. As a validation example, we evaluated the EM exposure of a realistic ear model illuminated by a 60 GHz plane wave. The EM field distribution over the entire ear was computed. By using a PCA regression, the unit vector field distribution normal to a model was estimated. The surface integral of time-averaged Poynting vector across the oriented surface of a model was approximated over a square- and a disk-shaped averaging surface of 1 cm^2.

Relative differences of 1.81 % and 0.92 % for TE and TM polarization, respectively, indicate that the APD_{av} depends only slightly on the shape of the averaging surface in the studied scenarios. However, the polarization of the EM field source has a more substantial impact (relative differences between TE and TM polarization are 13.11 % and 14 % for a square- and a disk-shaped averaging surface, respectively). Future work will consider wider range of exposure scenarios by extending the analysis to other frequency bands emerging for 5G/6G and by employing realistic radiation sources.

References

[1] International Commission on Non-Ionizing Radiation Protection (ICNIRP), "Guidelines for limiting exposure to electromagnetic fields (100 kHz to 300 GHz)," *Health Physics*, vol. 118, pp. 483–524, 2020. [Online]. Available: https://doi.org/10.1097/HP.0000000000001210

[2] "IEEE standard for safety levels with respect to human exposure to electric, magnetic, and electromagnetic fields, 0 Hz to 300 GHz," *IEEE Std C95.1-2019 (Revision of IEEE Std C95.1-2005/ Incorporates IEEE Std C95.1-2019/Cor 1-2019)*, pp. 1–312, 2019. [Online]. Available: https://doi.org/10.1109/IEEESTD.2019.8859679

[3] Y. Hashimoto, A. Hirata, R. Morimoto, S. Aonuma, I. Laakso, K. Jokela, and K. Foster, "On the averaging area for incident power density for human exposure limits at frequencies over 6 GHz," *Physics in Medicine and Biology*, vol. 62, no. 8, pp. 3124–3138, 2017. [Online]. Available: https://doi.org/10.1088/1361-6560/aa5f21

[4] A. Hirata, S. Kodera, K. Sasaki, J. Gomez-Tames, I. Laakso, A. Wood, S. Watanabe, and K. R. Foster, "Human exposure to radiofrequency energy above 6 GHz: review of computational dosimetry studies," *Physics in medicine & biology*, vol. 66, no. 8, p. 08TR01, 2021. [Online]. Available: https://doi.org/10.1088/1361-6560/abf1b7

[5] Y. Diao, E. A. R. Rashed, and A. Hirata, "Assessment of absorbed power density and temperature rise for nonplanar body model under electromagnetic exposure above 6 GHz," *Physics in medicine & biology*, vol. 65, no. 22, p. 224001, 2020. [Online]. Available: https://doi.org/10.1088/1361-6560/abbdb7

[6] G. Sacco and M. Zhadobov, "Variations of induced exposure levels at mmWaves in curved body parts," *IEEE Journal of Electromagnetics, RF and Microwaves in Medicine and Biology*, submitted.

[7] C. Sforza, G. Grandi, M. Binelli, D. G. Tommasi, R. Rosati, and V. F. Ferrario, "Age- and sex-related changes in the normal human ear," *Forensic Science International*, vol. 187, no. 1, pp. 110.e1–110.e7, 2009. [Online]. Available: https://doi.org/10.1016/j.forsciint.2009.02.019

[8] C. Gabriel, "Compilation of the dielectric properties of body tissues at RF and microwave frequencies," vol. Final Technical Report, 1996, pp. TR–1996–0037. [Online]. Available: https://doi.org/10.21236/ada303903

[9] H. Hoppe, T. DeRose, T. Duchamp, J. McDonald, and W. Stuetzle, "Surface reconstruction from unorganized points," *ACM Special Interest Group on Computer Graphics*, vol. 26, no. 2, p. 71–78, 1992. [Online]. Available: https://doi.org/10.1145/142920.134011

[10] K. Kim and M. Song, "Symmetric quadrature formulas over a unit disk," *Korean Journal of Computational & Applied Mathematics*, vol. 4, pp. 179–192, 1997. [Online]. Available: https://doi.org/10.1007/BF03011388

[11] M. Abramowitz and I. A. Stegun, *Handbook of Mathematical Functions With Formulas, Graphs, and Mathematical Tables*. Dover Publication, 1972, ch. 25.4.29.